Remote Sensing of Environment 160 (2015) 134–143

Contents lists available at ScienceDirect

Remote Sensing of Environment

journal homepage: www.elsevier.com/locate/rse

Uncertainty of remotely sensed aboveground biomass over an African tropical forest: Propagating errors from trees to plots to pixels

Qi Chen [a,*], Gaia Vaglio Laurin [b], Riccardo Valentini [b,c]

[a] Department of Geography, University of Hawai'i at Mānoa, 422 Saunders Hall, 2424 Maile Way, Honolulu, HI 96822, USA
[b] CMCC — Centro Mediterraneo sui i Cambiamenti Climatici, via Augusto Imperatore (Euro-Mediterranean Center for Climate Change), IAFENT Division, via Pacinotti 5, Viterbo, 01100, Italy
[c] Department for Innovation in Biological, Agro-food and Forest Systems, Tuscia University, Viterbo, 01100, Italy

ARTICLE INFO

Article history:
Received 9 August 2014
Received in revised form 10 January 2015
Accepted 13 January 2015
Available online 3 February 2015

Keywords:
Uncertainty
Error
Aboveground biomass
Carbon
Lidar
Tropical forests

ABSTRACT

Quantifying the uncertainty of the aboveground biomass (AGB) and carbon (C) stock is crucial for understanding the global C cycle and implementing the United Nations Program on Reducing Emissions from Deforestation and Forest Degradation (UN-REDD). The uncertainty analysis of remotely sensed AGB is tricky because, if validation plots or cross-validation is used for error assessment, the AGB of validation plots does not necessarily represent the actual measurements but estimates of the true AGB. Leveraging a recently published pan-tropical destructively measured tree AGB database, this study proposed a new method of characterizing the uncertainty of the remotely sensed AGB. The method propagates errors from tree- to landscape-level by considering errors in the whole workflow of the AGB mapping process, including allometric model development, tree measurements, tree-level AGB prediction, plot-level AGB estimation, plot-level remote sensing based biomass model development, remote sensing feature extraction, and pixel-level AGB prediction. Applying such a method to the tree AGB mapped using airborne lidar over tropical forests in Ghana, we found that the AGB prediction error is over 20% at 1 ha spatial resolution, larger than the results reported in previous studies for other tropical forests. The discrepancy between our studies and others reflects not only our focus on African tropical forests but also the methodological differences in our uncertainty analysis, especially in the aspect of comprehensively addressing more sources of uncertainty. This study also highlights the importance of considering the plot-level AGB estimate uncertainty when field plots are used to calibrate remote sensing based biomass models.

1. Introduction

Tropical forests contain ~50% of the aboveground carbon (C) in global vegetation (Hunter, Keller, Vitoria, & Morton, 2013), account for ~33% of terrestrial net primary productivity (Bonan, 2008), and play a crucial role in global C cycle and climate change (Grace, Mitchard, & Gloor, 2014). Tropical forests have also been experiencing intense pressure from land use changes such as deforestation and degradation (Berenguer et al., 2014). However, substantial uncertainty remains in estimating tropical forest C emissions from those human activities (Clark, Roberts, Ewel, & Clark, 2011). Because land use change is a patchy process (Ometto et al., 2014), accurately mapping the spatial distribution of tropical C stock and its dynamics is vital to reduce such uncertainty (Achard et al., 2014). Remote sensing is a promising technology to achieve this goal with its ability of providing synoptic view of the whole study area (Chen, 2013; DeFries et al., 2007).

Considerable efforts have been devoted to map tropical forest biomass at the landscape (e.g., Dubayah et al., 2010; Mascaro, Detto, Asner, & Muller-Landau, 2011; Vaglio Laurin et al., 2014), national (Asner et al., 2012), continental (Baccini, Laporte, Goetz, Sun, & Dong, 2008; Goetz et al., 2009), and even cross-continental (Baccini et al., 2012; Saatchi et al., 2011) scales using remote sensing technology. However, accompanying with the sheer number of biomass mapping studies is the substantial variations among the various estimates of biomass and C stock (Houghton, Lawrence, Hackler, & Brown, 2001; Mitchard et al., 2013; Ometto et al., 2014), which makes it difficult to choose a product for making forest management decision in mitigating the impacts of climate change.

Central to understanding the quality of remotely sensed biomass and C maps is to quantify the uncertainty of the estimated biomass from remote sensing based models (Lu et al., 2014; Wang et al., 2009). Root mean square errors (RMSE) is the most common statistic to characterize the error of remote sensing based biomass models (Zolkos, Goetz, & Dubayah, 2013) and it is calculated by comparing model prediction to "true" biomass over a sample of forest plots. One of the key distinctions of mapping biomass, compared to mapping many other vegetation attributes such as tree height and basal area, is that the ground truth biomass for calibrating a remote sensing model has rarely been directly measured (Clark & Kellner, 2012). Instead, it is estimated using allometric models with other tree- and site-level attributes, such

* Corresponding author. Tel.: +1 808 956 3524; fax: +1 808 956 3512.
E-mail address: qichen@hawaii.edu (Q. Chen).

http://dx.doi.org/10.1016/j.rse.2015.01.009
0034-4257/

as DBH (diameter at breast height), tree height and wood density, as predictors. Both the allometric model predictions and tree attributes could have errors, which can be propagated to the plot-level biomass estimates and thus affect the uncertainty of the biomass estimation from a remote sensing based model.

Remotely sensed biomass mapping involves the combined use of two types of models: 1) allometric models for estimating tree- and plot-level biomass using tree attributes such as DBH, tree height, and wood density, 2) models for predicting pixel-level biomass using remote sensing derived variables. Both models have parameters, the uncertainty of which could lead to uncertainty in biomass estimation. The omission of model parameter uncertainty will underestimate the biomass prediction uncertainty (Yanai et al., 2010).

Overall, the uncertainty assessment of remotely sensed biomass needs to consider errors and uncertainty in the whole process of upscaling biomass from tree to plot and landscape levels, including those related to field measurements, allometric models, lidar data, and statistical modeling. Many of these issues have been investigated in the past (see McRoberts and Westfall (2014) for a recent review), especially from the perspective of estimating the mean statistic of forest attributes (e.g., volume, biomass) and its uncertainty over a large area (e.g., Berger, Gschwantner, McRoberts, & Schadauer, 2014; Breidenbach, Antón-Fernández, Petersson, McRoberts, & Astrup, 2014; Gregoire et al., 2010; McRoberts & Westfall, 2014; Ståhl, Heikkinen, Petersson, Repola, & Holm, 2014). However, only a few studies (e.g., Gonzalez et al., 2010) have quantified the biomass uncertainty at the pixel level when remote sensing data are used for biomass estimation.

The main goal of this study is to develop a methodology to assess the uncertainty of remotely sensed aboveground biomass (AGB) at the pixel level over western African tropical forests in Ghana with a synergistic use of field data, airborne lidar, allometric modeling, and remote sensing based biomass modeling. This study addresses these questions: 1) what the errors associated with allometric models and lidar-based biomass models are, 2) how the errors of tree measurements collected in a forest plot will be propagated to the biomass estimates at the tree- and plot-level when an allometric model is used to predict biomass, 3) how the errors in lidar metrics will be propagated to AGB prediction, 4) how the plot-level AGB errors affect the lidar-biomass AGB modeling and prediction errors, and 5) what the major error sources in AGB prediction at the tree- and pixel levels are.

2 . Study area and data

2.1. Study area

Our study area transverses transects along a ~100 km latitudinal gradient in Southwest Ghana close to the border with Ivory Coast (Fig. 1). These transects are along the orbits of ICESat and were mapped with airborne lidar with width of ~250 m to 750 m. The first group of transects is located in the Bia Conservation Area that comprises of Bia National Park (BNP) and Bia Resource Reserve (BRR). The area covers the transition between two of Ghana's forest types, Moist Evergreen forest in the south and Moist Semi-deciduous forests in the north. BRR was logged in 1980–90, and possibly even after; it can be impacted by natural (fire, elephants' damages) and illegal human-related disturbance. BNP has a better protection status and no logging records, but fires, elephants' damages and illegal access could occur. The second group of transects is located in the Dadieso Forest Reserve (DFR), which lies south of the Bia Conservation Area but north of Boin river Forest Reserve and Disue Forest Reserve. The vegetation of the reserve is transitional between Moist Evergreen and Wet Evergreen types. DFR was illegally logged and surrounded by communities and coffee farms; furthermore it has swampier characteristics, and flooding can represent a frequent natural disturbance.

2.2. Field measurements

Along the ICESat orbits, the field plots were set up at the footprints of GLAS laser shots with the goal of upscaling biomass from local to regional scale. The GLAS waveforms were first screened to exclude the shots that are saturated or contaminated by clouds (Chen, 2010). So, the plots can be considered as a quasi-transect sample of the forests. The field plots have a square shape of 40 m by 40 m. For each plot, DBH, tree height, and species information was collected for all trees having DBH > 20 cm. For trees with DBH in the 10–20 cm range, the same information was collected in subplots of 400 m^2. We did not measure wood density but use estimates from Chave et al. (2009). A total of 36 field plots are used in our analysis (13 in BNP, 3 in BRR, and 20 in DFR).

2.3. Airborne lidar data

The study area was surveyed by an airborne campaign in March 2012 over pre-defined flight lines covering the field plots, using a Pilatus PC-6 Porter aircraft equipped with lidar and hyperspectral sensors and a digital camera for aerial photographs. The lidar sensor ALTM GEMINI (Optech Ltd.), characterized by a 1064 nm laser wavelength and able to record up to 4 range measurements, was operated 650–850 m above ground level. The minimum laser density was set to 11 points/m^2. The positional errors of the laser returns in the horizontal and vertical dimensions were lower than 0.27 m.

The raw all-returns point cloud was processed using the Toolbox for Lidar Data Filtering and Forest Studies (TIFFS) (Chen, 2007) to derive a range of metrics for AGB estimation from each plot, including: mean height, quadratic mean height, standard deviation height, height bins at 5 m intervals and 10% percentile heights. TIFFS used the ground returns identified by the data provider to generate a DTM (Digital Terrain Model) and calculated the relative height above terrain of each laser return by subtracting the corresponding DTM elevation from its original Z value. The lidar metrics were derived using the relative height of all laser points. We generated lidar metric maps of 40 m by 40 m cell size, equivalent to the field plot size.

2.4. Pan-tropical tree AGB database

We developed an allometric model from a pan-tropical destructive tree database compiled by Chave et al. (2014) (see http://chave.ups-tlse.fr/pantropical_allometry.htm) to fully characterize the tree AGB prediction errors. This database (called Chave14 hereinafter) includes a total of 4004 trees from 53 undisturbed and five secondary forest sites across tropics in Latin America, Southeast Asia, and Africa. The tree measurements include DBH (cm), tree height (m), wood specific gravity or wood density (g/cm^3), and total oven-dry AGB (kg).

3 . Methods

3.1. Errors of tree-level AGB prediction

We first developed a pan-tropical allometric model from the Chave14 tree database. An allometric model is used to predict AGB using other easily measurable tree attributes such as DBH, tree height, and wood density (denoted as $\boldsymbol{x}$ as a whole). The model is usually calibrated from a sample of trees for which AGB has been measured via destructive sampling and $\boldsymbol{x}$ has been obtained by direct measurements or estimation:

$$E(B_{tree}|\boldsymbol{x}) = f_{tree}(\boldsymbol{\beta}, \boldsymbol{x}) \quad (1)$$

$$\mathrm{var}(B_{tree}|\boldsymbol{x}) = {\sigma_{\varepsilon,tree}}^2 \quad (2)$$

where $E()$ and var() represent the expectation and variance of a variable; f_{tree} is the allometric model with parameter(s) $\boldsymbol{\beta}$ to predict tree

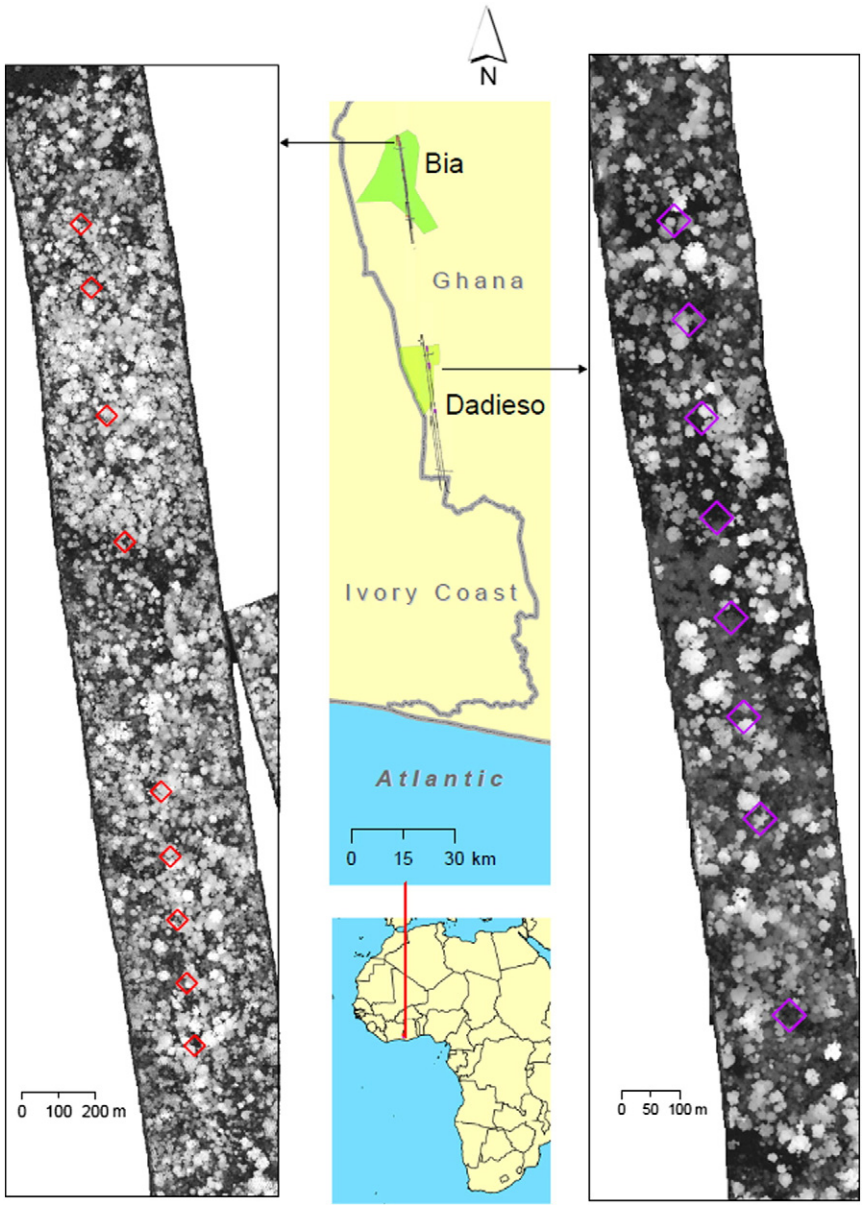

Fig. 1. The study area (transects in the middle upper figure), lidar transects (left and right figures as examples), and 40 by 40 m field plots (see squares over the lidar transects as examples).

AGB (i.e., B_{tree}); ${\sigma_{\varepsilon,tree}}^2$ is the variance of AGB for trees with attributes $\boldsymbol{x}$. Note that $\boldsymbol{\beta}$ and $\boldsymbol{x}$ could be scalars or vectors $[\beta_1, \beta_2, \ldots]$ and $[x_1, x_2, \ldots]$.

Instead of using the log-transformation method (e.g., Chave et al., 2014), we developed a Generalized Least Squares (GLS) based approach that can directly model AGB without the need of bias correction (Brown, Gillespie, & Lugo, 1989).

$$B_{tree} = f_{tree}(\boldsymbol{\beta}, \boldsymbol{x}) + \varepsilon_{tree} \tag{3}$$

$$\varepsilon_{tree} = g(\boldsymbol{\beta}, \boldsymbol{x}, \boldsymbol{\theta})\xi \tag{4}$$

where ε_{tree} is the residual between the measured and estimated AGB for a tree; $g(\boldsymbol{\beta}, \boldsymbol{x}, \boldsymbol{\theta})$ is a function of $\boldsymbol{x}$ with parameters $\boldsymbol{\beta}$ and $\boldsymbol{\theta}$ to model residuals; ξ is a standard normal variable. The common forms for g are linear, proportional, or power functions of $f(\boldsymbol{\beta}, \boldsymbol{x})$. We found that the residuals from OLS model fitting increase with tree size and thus used the proportional model:

$$g(\boldsymbol{\beta}, \boldsymbol{x}, \boldsymbol{\theta}) = \theta f_{tree}(\boldsymbol{\beta}, \boldsymbol{x}) \tag{5}$$

Note that, since ξ is a standard normal variable, the standard deviation of the residuals ε_{tree} is:

$$\sigma_{\varepsilon,tree} = \theta f_{tree}(\boldsymbol{\beta}, \boldsymbol{x}) \tag{6}$$

We used the same model form as the one in Chave et al. (2014) for $f_{tree}(\boldsymbol{\beta}, \boldsymbol{x})$:

$$f_{tree}(\boldsymbol{\beta}, \boldsymbol{x}) = \beta_1 \left(\rho D^2 H\right)^{\beta_2} \tag{7}$$

where ρ, D, and H are wood density, DBH, and tree height, respectively. With the choice of such a model, $\boldsymbol{\beta} = [\beta_1, \beta_2]$ and $\boldsymbol{x} = [\rho, D, H]$. The detailed steps of fitting the allometric model using GLS are described in Appendix 1. The model parameters (denoted as $\hat{\beta}_1$, $\hat{\beta}_2$, and $\hat{\theta}$) were estimated by assuming no measurement errors exist in the Chave14 dataset.

An important distinction has to be made between the AGB estimation errors of 1) a tree from the sample for model development (i.e., from the Chave14 tree database) and 2) a *new* tree (i.e., not in the Chave14 database) for which AGB is to be predicted. The AGB

error of the former is $\sigma_{\varepsilon,tree}$. However, the error of the latter is called tree AGB *prediction error*, which is always larger than $\sigma_{\varepsilon,tree}$ due to 1) uncertainty in model parameters, and 2) errors in the measurements of tree attributes $\boldsymbol{x}$. The prediction error is what we should be concerned about when the allometric model is applied to a new place for biomass estimation. The next two subsections 3.1.1 and 3.1.2 discuss the AGB prediction errors of the allometric model.

3.1.1. Errors of AGB prediction associated with model parameters

When the estimated parameters $\hat{\beta}_1$ and $\hat{\beta}_2$ are plugged into Eq. (7) to estimate the AGB of a *new* tree, we get

$$\hat{B}_{tree} = \hat{\beta}_1 \left(\rho D^2 H\right)^{\hat{\beta}_2} \tag{8}$$

The estimated tree AGB, $\hat{B}_{tree}$, is uncertain due to the uncertainty in the estimates of parameters. The AGB prediction error caused by model parameters' uncertainty is denoted as $\sigma_{f,tree}$. With linear approximation (see, e.g., Section 2.3 of Bates and Watts (1988)), $\sigma_{f,tree}$ can be calculated as in Appendix 2.

Note that $\hat{B}_{tree}$ essentially represents the *mean* (or expectation of) biomass of trees with the same attributes $\boldsymbol{x}$. $\sigma_{f,tree}$ characterizes the "standard error" of the *mean*, not the error of *individual* tree AGB. If $\hat{B}_{tree}$ is used as the AGB estimate at the individual level, its error is larger:

$$\sigma_{tree}^2 = \sigma_{\varepsilon,tree}^2 + \sigma_{f,tree}^2 \tag{9}$$

where $\sigma_{\varepsilon,tree}^2$ is calculated using Eq. (6) for the new tree; σ_{tree} is the tree AGB prediction error of the allometric model.

3.1.2. Errors of AGB prediction associated with tree attributes

The σ_{tree} shown in Eq. (9) is derived based on the assumption that no errors exist in the measurements of *new* tree attributes $\boldsymbol{x}$. In fact, tree attributes $\boldsymbol{x}$ can be measured or estimated with errors. Because both $\sigma_{\varepsilon,tree}$ and $\sigma_{f,tree}$ are dependent on $\boldsymbol{x}$, the errors in $\boldsymbol{x}$ will be propagated to the tree AGB estimates. We found that, when the $\boldsymbol{x}$ errors are considered, the tree AGB prediction error σ_{tree} is as follows (see Appendix 3):

$$\sigma_{tree}^2 = \sigma_{\varepsilon,tree}^2 + \sigma_{f,tree}^2 + \left(\hat{\theta}^2 + 1\right) \mathrm{var}\left(f_{tree}\left(\hat{\boldsymbol{\beta}}, \boldsymbol{x}\right)\right) + \mathrm{var}\left(\sigma_{f,tree}\right) \tag{10}$$

where $\mathrm{var}\left(f_{tree}\left(\hat{\boldsymbol{\beta}}, \boldsymbol{x}\right)\right)$ can be estimated using first-order Taylor Series expansion (Gertner, Cao, & Zhu, 1995) and $\mathrm{var}(\sigma_{f,tree})$ can be estimated using Monte-Carlo simulation (Gonzalez et al., 2010). Note that when tree measurements $\boldsymbol{x}$ are error-free, both $\mathrm{var}\left(f_{tree}\left(\hat{\boldsymbol{\beta}}, \boldsymbol{x}\right)\right)$ and $\mathrm{var}(\sigma_{f,tree})$ are equal to zero, making Eq. (10) equivalent to Eq. (9). We denote $\left(\hat{\theta}^2 + 1\right) \mathrm{var}\left(f_{tree}\left(\hat{\boldsymbol{\beta}}, \boldsymbol{x}\right)\right) + \mathrm{var}\left(\sigma_{f,tree}\right)$ as $\sigma_{x,tree}^2$ to indicate that the relevant tree AGB prediction errors are caused by errors in $\boldsymbol{x}$.

3.2. Errors of plot-level AGB estimated using field data

Eqs. (8)–(10) can predict tree AGB and errors for the field plots used for developing remote sensing based biomass models. The predicted plot-level AGB density $\hat{B}_{plot}$ of a plot is the sum of individual tree $\hat{B}_{plot}$ divided by the plot area s (m^2):

$$\hat{B}_{plot} = \sum_{i=1}^{n_{tree,plot}} \hat{B}_{tree,i}/s \tag{11}$$

where $n_{tree,plot}$ is the number of trees within the plot; $\hat{B}_{tree,i}$ is calculated using Eq. (8). Note that since the minimum DBH of the tree measurements of our field plots in Ghana is 10 cm, $\hat{B}_{plot}$ quantifies the oven-dry aboveground biomass density for live trees of DBH > 10 cm. The $\hat{B}_{plot}$ in Eq. (11) has a unit of kg/m^2, which can be converted to Mg/ha by multiplying a factor of 10.

The standard deviation of $\hat{B}_{plot}$ for the plot is:

$$\sigma_{\hat{B}_{plot}} = \sqrt{\sum_{i=1}^{n_{tree,plot}} \sigma_{tree,i}^2 / s} \tag{12}$$

where $\sigma_{tree,i}$ is the tree AGB error calculated using either Eq. (9) or Eq. (10). Note that this formula assumes that the errors among trees on the same plot are independent. McRoberts and Westfall (2014) found that such an assumption is reasonable for estimating the mean stem tree volume over large areas.

3.3. Errors of AGB estimates from lidar-based biomass model

Using the plot-level AGB estimates $\hat{B}_{plot}$ and lidar metrics (denoted as $\boldsymbol{z}$), a lidar-based biomass prediction model can be developed:

$$\hat{B}_{plot} = f_{plot}(\boldsymbol{\varphi}, \boldsymbol{z}) + \varepsilon_{plot} \tag{13}$$

where $\boldsymbol{\varphi}$ is the lidar-biomass model parameter(s); ε_{plot} is the residual term of the model. The caret (^) is used in this model formulation because the response variable, plot-level AGB, cannot be considered to be an observation without error, but rather an estimate obtained from application of the allometric model.

We chose the multiplicative power models (Chen, Vaglio Laurin, Battles, & Saah, 2012; Vaglio Laurin et al., 2014) for biomass estimation:

$$f_{plot}(\boldsymbol{\varphi}, \boldsymbol{z}) = \varphi_0 z_1^{\varphi_1} z_2^{\varphi_2} \ldots z_m^{\varphi_m} \tag{14}$$

where z_1, z_2, and z_m are different lidar metrics. With such a model form, $\boldsymbol{\varphi} = [\varphi_0, \varphi_1, \varphi_2, \ldots, \varphi_m]$ and $\boldsymbol{z} = [z_1, z_2, \ldots, z_m]$.

We found that ε_{plot} increases with plot-level AGB density when OLS was used for model fitting. Therefore, we modeled the residuals directly:

$$\varepsilon_{plot} = k f_{plot}(\boldsymbol{\varphi}, \boldsymbol{z}) \xi \tag{15}$$

where k is a parameter, ξ is a standard normal variable. Correspondingly, the standard deviation of the lidar-biomass model residuals (i.e., ε_{plot}) is:

$$\sigma_{\varepsilon,plot} = k f_{plot}(\boldsymbol{\varphi}, \boldsymbol{z}) \tag{16}$$

For the lidar-based biomass model, the AGB of a field plot is not an actual measurement but an estimate (Fig. 2). The estimate $\hat{B}_{plot}$ is different from the true AGB density B_{plot} for a plot. If the uncertainty of $\hat{B}_{plot}$ is not considered in model fitting, the standard deviation of the model residuals (i.e., $\sigma_{\varepsilon,plot}$) will be underestimated. To address this issue, we modified the GLS method as shown in Appendix 4. The estimated parameters are denoted as $\hat{\boldsymbol{\varphi}}$ and $\hat{k}$.

Once the lidar-based biomass model has been calibrated, Eq. (14) can be used to predict AGB density $\hat{B}_{pix}$ for pixels that have equivalent areas to the field plots. As a reminder, similar to the tree-level allometric model, Eq. (14) is to predict the expected (or mean) biomass of pixels with the same lidar metrics $\boldsymbol{z}$. This predicted mean has a standard error caused by the uncertainty in the estimated model parameters $\hat{\boldsymbol{\varphi}}$. We denote this error as $\sigma_{f,pix}$.

When lidar metrics $\boldsymbol{z}$ has no errors, the predicted AGB at the pixel-level has an error of:

$$\sigma_{pix}^2 = \sigma_{\varepsilon,pix}^2 + \sigma_{f,pix}^2 \tag{17}$$

where $\sigma_{\varepsilon,pix}$ is calculated using Eq. (16) for the pixel; σ_{pix} is the AGB prediction error of the lidar-based biomass model for a pixel.

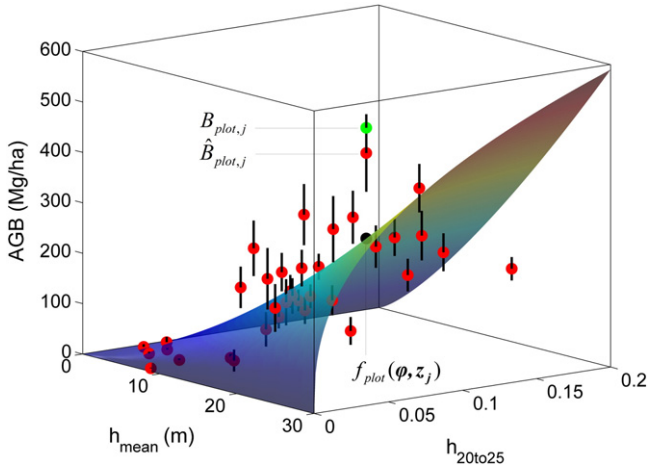

Fig. 2. Modeling the residuals of the lidar-based biomass model. Red dots are estimated plot-level AGB density $\hat{B}_{plot}$. Black lines are standard deviation of $\hat{B}_{plot}$. The green dot is a hypothetical value of the true AGB, B_{plot}, for plot j. The dark dot is the predicted AGB from lidar $f_{plot}(\boldsymbol{\varphi}, \boldsymbol{z})$ for plot j. The curved surface is the lidar-based AGB prediction function, Eq. (21).

Similar to the derivations for tree-level AGB prediction errors (see Appendix 3), we found that, when the lidar metrics $\boldsymbol{z}$ of a pixel has errors, the error ${\sigma_{pix}}^2$ is:

$$ {\sigma_{pix}}^2 = {\sigma_{\varepsilon,pix}}^2 + {\sigma_{f,pix}}^2 + \left(\hat{k}^2+1\right)\mathrm{var}\left(f_{plot}(\hat{\boldsymbol{\varphi}},\boldsymbol{z})\right) + \mathrm{var}\left(\sigma_{f,pix}\right) \quad (18) $$

where $\mathrm{var}\left(f_{plot}(\hat{\boldsymbol{\varphi}},\boldsymbol{z})\right)$ again can be estimated using first-order Taylor Series expansion and $\mathrm{var}(\sigma_{f,pix})$ can be estimated using Monte-Carlo simulation. When lidar metrics $\boldsymbol{z}$ have no errors, both $\mathrm{var}\left(f_{plot}(\hat{\boldsymbol{\varphi}},\boldsymbol{z})\right)$ and $\mathrm{var}(\sigma_{f,pix})$ are equal to zeros, which implies that the above two equations are equivalent in such a situation. The sum of the last two terms of the right hand side of Eq. (18), $\left(\hat{k}^2+1\right)\mathrm{var}\left(f_{plot}(\hat{\boldsymbol{\varphi}},\boldsymbol{z})\right) + \mathrm{var}\left(\sigma_{f,pix}\right)$, are caused by errors in lidar metrics $\boldsymbol{z}$ and thus are denoted as ${\sigma_{z,pix}}^2$.

3.3.1. Selection of lidar metrics for model fitting

Considerable correlations exist among the individual lidar metrics. We used a two-step procedure to select the most relevant ones for biomass prediction. First, we did a log-transformation of both the response and predictor variables, which turned the multiplicative power model to a linear model. Then forward stepwise regression was used to select the statistically significant lidar metrics. The inference of the model parameters at the log-scale is not exactly the same as the one in the original scale. To avoid the exclusion of useful lidar metrics, we set the p-values for variables entering and removing from the model to be 0.1 and 0.2, respectively, higher than the common values of 0.05 and 0.1. Second, we used the lidar metrics selected by stepwise regression to develop the multiplicative power model using nonlinear model fitting technique. The p-values of the individual variables in the multiplicative power model were checked and, any statistically insignificant variables (p-value > 0.05) were removed and the models are refitted. The second step can be iterated until all variables are statistically significant (Vaglio Laurin et al., 2014). After the lidar metrics were selected, they were used in the GLS method for parameter estimation and error characterization (see Eqs. 13–18).

3.4. Evaluating the impacts of field measurement errors and lidar metric errors

The uncertainty analysis of the AGB maps derived from field measurements and remote sensing data requires information about the errors of tree attributes $\boldsymbol{x}$ and lidar metrics $\boldsymbol{z}$. We do not have direct measurements of these errors, so we rely on the previous studies to set up the error estimates for our analysis. Throughout the text, we refer to the standard deviation of an estimate or measurements as *absolute error* while the standard deviation divided by the estimate or measurement mean as *relative error*. Note that here we ignore the bias that could exist in the tree measurements or lidar data. For wood density, we followed Chave et al. (2004) and set the relative errors to 10%. For tree height, Chave et al. (2004) used a relative error of 10%, which is higher than 7.8% of temperate forest used by Phillips, Brown, Schroeder, and Birdsey (2000). However, Hunter et al. (2013) found the precision of tropical tree height measurement could range from 3% to 20% of the tree height. Here, we adopted the upper limit, 20%, in our analysis. Chave et al. (2004) used a sum of two normal distributions to characterize the DBH error. We simplified this to set the relative error of DBH to be 5%, which is higher than 2–3% used in temperate forests (Gonzalez et al., 2010; Phillips et al., 2000) and considers the difficulty of measuring DBH in tropical forests. We will introduce the errors of lidar metrics $\boldsymbol{z}$ in the next section after we have determined the remote sensing biomass model.

4 . Results and discussion

4.1. Errors of tree-level AGB prediction

The GLS estimates of the allometric model parameters are: $\hat{\beta}_1 = 0.0704$, $\hat{\beta}_2 = 0.9701$, and $\hat{\theta} = 0.3777$. Therefore, the pan-tropical allometric model for predicting tree AGB is:

$$ \hat{B}_{tree} = 0.0704\left(\rho D^2 H\right)^{0.9701} \quad (19) $$

where ρ is in g/cm^3, D is in cm, H is in m, and $\hat{B}_{tree}$ is in kg.

The equation for $\sigma_{\varepsilon,tree}$ is:

$$ \sigma_{\varepsilon,tree} = 0.3777\hat{B}_{tree} \quad (20) $$

This indicates that the relative AGB error caused by $\sigma_{\varepsilon,tree}$ is about 37.8%. With a database of fewer trees, Chave et al. (2004) reported a smaller relative $\sigma_{\varepsilon,tree}$ error of 31.3%. The larger $\sigma_{\varepsilon,tree}$ here is mainly related to the difference between the Chave14 database and the one used in Chave et al. (2004).

Besides $\hat{B}_{tree}$ and $\sigma_{\varepsilon,tree}$, we also calculated the model parameter related AGB error $\sigma_{f,tree}$ and tree attributes x related AGB error $\sigma_{x,tree}$ for all trees ($n = 1191$) of the 36 field plots in Ghana. The equation to calculate $\sigma_{f,tree}$ is presented in Appendix 5. We found that, if we additionally consider the two other error sources (i.e., $\sigma_{f,tree}$ and $\sigma_{x,tree}$), the relative error of tree AGB prediction increases from 37.8% to 50.0%. This is slightly higher than the 47% value reported in Chave et al. (2004), mostly caused by an increase in our $\sigma_{\varepsilon,tree}$.

The relative AGB prediction error caused by $\sigma_{f,tree}$ alone is very small ($\sigma_{f,tree}/\hat{B}_{tree} = 0.74\%$), mainly because the sample size is large ($n = 4004$) for the Chave14 tree database and the variance–covariance of model parameters are inversely related to the sample size. We did simulations to reduce the sample size from 4004 to 400 and 40. The results showed that the relative AGB prediction error related to $\sigma_{f,tree}$ increases from 0.74% to 2.52% and 5.69%, respectively. Thus, using a large tree database such as Chave14 for calibrating the allometric model is valuable to reduce AGB prediction error related to model parameters.

For AGB prediction at the tree-level, $\sigma_{\varepsilon,tree}$, $\sigma_{f,tree}$, and $\sigma_{x,tree}$ contribute to 57.59% $(=\sigma_{\varepsilon,tree}{}^2/\sigma_{tree}{}^2)$, 0.02% $(=\sigma_{f,tree}{}^2/\sigma_{tree}{}^2)$, and 42.39% $(=\sigma_{x,tree}{}^2/\sigma_{tree}{}^2)$ of the total error σ_{tree}, respectively. Therefore, for our field plots in Ghana, the tree AGB prediction errors were dominated by model prediction residuals ($\sigma_{\varepsilon,tree}$) and errors in tree attributes $\boldsymbol{x}$ ($\sigma_{x,tree}$).

4.2. Errors of plot-level AGB estimates derived from field data

The previous section shows that the tree-level AGB error is 50.0% when all error sources are considered. At the plot-level, the corresponding AGB density $\hat{B}_{plot}$ error reduces to 19.5%. The cause of the smaller relative AGB error at the plot level is mathematical: the plot-level AGB standard deviation $\sigma_{\hat{B}_{plot}}$ involves the square root of sum (Eq. 12) while AGB mean $\hat{B}_{plot}$ directly uses the sum in the numerator (Eq. 11). Hence, the relative error, $\sigma_{\hat{B}_{plot}}$ divided by $\hat{B}_{plot}$, usually has a negative relationship with the number of trees within a plot (Chave et al., 2004).

4.3. Errors of pixel-level AGB estimates from lidar-based biomass model

Based on the feature selection method introduced in 3.3.1, the lidar-based biomass model developed from the 36 field plots in Ghana is:

$$\hat{B}_{pix} = 14.55 h_{mean}{}^{1.27} h_{20to25}{}^{0.38} \tag{21}$$

where h_{mean} is the mean height of laser points; h_{20to25} is the proportion of laser points within 20 to 25 m. The lidar metrics were calculated using all returns including those on the ground. This model was developed with the assumption of spatial independence among model prediction residuals. The experimental variogram calculated from the model prediction residuals did not show obvious spatial autocorrelation, which suggests that the above model can be used to predict pixel-level AGB and its errors without bias (Barrett, Galbally, & Graetz, 2001).

The equation for $\sigma_{\varepsilon,pix}$ is:

$$\sigma_{\varepsilon,pix} = 0.479 \hat{B}_{pix} \tag{22}$$

This means that, at the plot- or pixel-level, the relative AGB prediction error due to lidar-biomass model residuals is 47.9%.

Using the 40-m maps of lidar metrics h_{mean} and h_{20to25}, we produced maps of $\hat{B}_{pix}$ and $\sigma_{\varepsilon,pix}$ of the same spatial resolution. Besides, we calculated the pixel-level model parameter related AGB error $\sigma_{f,pix}$ and lidar metrics related AGB error $\sigma_{z,pix}$ (Fig. 3). We calculated $\sigma_{z,pix}$ by assuming the relative errors of both h_{mean} and h_{20to25} to be 10%. The uncertainty in lidar metrics are mainly related to the errors in extracting ground elevation from laser points as well as the sampling nature of lidar data. Asner et al. (2012) used an error estimate of 5% for lidar height metrics. We set the error estimate arbitrarily higher, simply for the purpose of testing how much AGB prediction errors can be caused by lidar metrics errors in a worse scenario.

At the pixel level, we found that the relative AGB prediction error caused by $\sigma_{f,pix}$ and $\sigma_{z,pix}$ are 16.2% and 16.0%, respectively ($\sigma_{f,pix}/\hat{B}_{pix} = 16.2\%, \sigma_{z,pix}/\hat{B}_{pix} = 16.0\%$). Recall that if only $\sigma_{\varepsilon,pix}$ is considered, the relative AGB prediction error is 47.9%. When both $\sigma_{f,pix}$ and $\sigma_{z,pix}$ are additionally considered, the total relative AGB prediction error increases to 54.1%. $\sigma_{\varepsilon,pix}$, $\sigma_{f,pix}$, and $\sigma_{z,pix}$ contribute to 80.5% $(=\sigma_{\varepsilon,pix}{}^2/\sigma_{pix}{}^2)$, 10.6% $(=\sigma_{f,pix}{}^2/\sigma_{pix}{}^2)$, and 8.8% $(=\sigma_{z,pix}{}^2/\sigma_{pix}{}^2)$ of the total error σ_{pix}, respectively. So, when the lidar-biomass model was applied to the study area, the dominant error source is the AGB error related to model residuals (i.e., $\sigma_{\varepsilon,pix}$). Note that the error related to model parameters, $\sigma_{f,pix}$, is no more negligible as in the tree allometric model. This is because the sample size for developing the lidar-biomass model ($n = 36$) is much smaller than the sample size for developing the allometric model ($n = 4004$).

4.4. Analysis of the remotely sensed AGB prediction errors

When all the error sources are considered, the previous section indicated that the relative AGB prediction error at the pixel-level, $\sigma_{pix}/\hat{B}_{pix}$, is 54.1%, which seems high. Next, we discuss different error sources and see whether the pixel-level relative AGB prediction error can be reduced and, if yes, how.

First, the large pixel-level AGB errors are partially caused by the fact that we considered the errors in measuring tree attributes $\boldsymbol{x}$ or estimating the lidar metrics $\boldsymbol{z}$ of field plots. If we assume that tree attributes were measured without errors, the pixel-level relative AGB prediction error reduces from 54.1% to 51.9%. If we further assume the lidar metrics are error-free as well, the AGB error reduces to 49.4%. Overall, the errors in tree measurements and lidar metrics contributed only a small portion of the total errors, especially considering that we intentionally set the errors in tree measurements and lidar metrics larger than those from most previous studies. Therefore, it is unlikely that improving the tree measurements and lidar data processing skills upon the state-of-the-art will dramatically reduce the pixel-level AGB relative error.

Another error source is related to the lidar-biomass model parameter uncertainty. As indicated in Appendix 2, $\sigma_{f,pix}$ is inversely related to the number of field plots. Recall that the pixel-level AGB relative error is 49.4% if no errors exist in tree measurements and lidar metrics. We created bootstrap samples from the 36 field plots and found that the error reduces slightly from 49.4% to 47.3%, 46.7%, and 46.6% when bootstrap sample sizes of field plots are 100, 200, and 500, respectively. Thus, collecting a large number of field plots does not have a large impact on $\sigma_{f,pix}$ either.

At the pixel level, $\sigma_{\varepsilon,pix}$ contributes about 80% of the total AGB prediction error. The corresponding relative AGB prediction error, $\sigma_{\varepsilon,pix}/\hat{B}_{pix}$, is 47.9%. $\sigma_{\varepsilon,pix}/\hat{B}_{pix}$ is also known as the relative RMSE when RMSE is calculated using calibration plots instead of separate validation or test plots (Zolkos et al., 2013). Our relative RMSE value is similar to the one from a separate study we did in Sierra Leone (Vaglio Laurin et al., 2014) but it is among the highest compared to those reported for other tropical forests (Zolkos et al., 2013). Smaller relative RMSEs can be obtained if we have larger field plots or aggregate the biomass maps to coarser resolutions. However, our simulation and analysis (details not shown due to space limitation) indicated that, with either approach, the relative AGB prediction error $\left(\sigma_{pix}/\hat{B}_{pix}\right)$ is larger than 20% at 1 ha spatial scale. Several recent studies (Asner & Mascaro, 2014; Zolkos et al., 2013) stated that the uncertainty of lidar-based AGB mapping can reach 10% at the 1 ha spatial resolution. The divergent results between ours and those are not only related to our focus on African tropical forests but also because we are using a different approach for uncertainty analysis, especially in the aspect of comprehensively addressing more sources of uncertainty.

4.5. Difference between our error analysis method and conventional ones

A common practice to evaluate remotely sensed AGB prediction error is to set aside validation field plots or use cross-validation for accuracy assessment. Such methods are legitimate if the AGB of the validation plots are directly measured. Unfortunately, directly measuring tree AGB for forest plots is extremely labor-intensive and thus rarely carried out (Asner & Mascaro, 2014; Clark & Kellner, 2012). Error propagation methods (Chave et al., 2004; Gonzalez et al., 2010), as used in this study, represent a fundamentally different approach to characterize the errors of the remotely sensed AGB. If the conventional error assessment method using validation plots are considered to be retrospective,

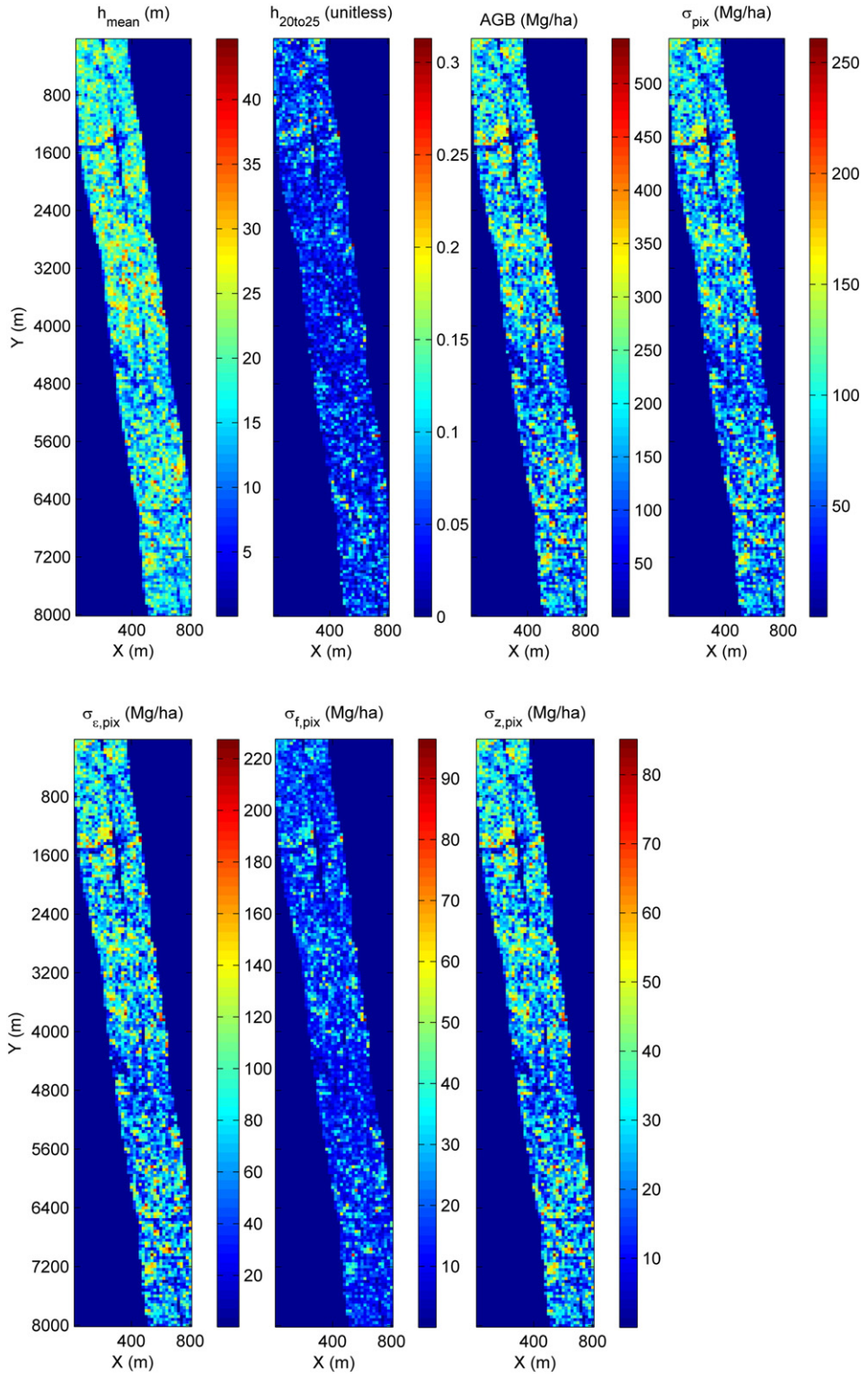

Fig. 3. Maps of lidar metrics, AGB, and errors. h_{mean} and h_{20to25} are two lidar metrics. AGB is the mapped aboveground biomass, σ_{pix} is the pixel-level AGB error, $\sigma_{\varepsilon,pix}$, $\sigma_{f,pix}$, and $\sigma_{z,pix}$ are errors related to lidar-biomass model residuals, model parameters, and lidar metrics, respectively.

the error propagation method we are using is forward-looking. The key of the conventional error assessment method is the true AGB measurements of the validation field plots while the key of the error propagation method is the true AGB measurements of the trees used for developing the allometric method. So, it is impossible for us to propose our method if destructive tree AGB databases such as Chave14 were not released publicly.

Error propagations can be done via either Monte-Carlo simulations (McRoberts & Westfall, 2014) or first-order Taylor linear approximation as in this study. The advantage of the approximation approach lies in its

computation efficiency, but the estimated model parameter errors might differ from their true values for nonlinear models. We evaluated the parameter curvature issue (Bates & Watts, 1988) and found that it is negligible for both the tree-level allometric model and the lidar-based biomass model.

4.6. Impacts of plot-level AGB uncertainty on lidar-based AGB modeling and prediction

In Section 4.2, we showed that the plot-level AGB uncertainty is 19.5% when the plot-level AGB is upscaled from tree AGB values (for the case that all the tree-level errors related to allometric model residuals, allometric model parameters, and tree measurements are considered). Unlike our approach (see Appendix 4), most previous studies did not consider the plot-level AGB uncertainty in remote sensing biomass modeling. If this type of error is not considered in our study, the relative AGB error related to the lidar-biomass model residuals $\left(\sigma_{\varepsilon,pix}/\hat{B}_{pix}\right)$ will be 41.9% instead of 47.9%; the total pixel-level relative AGB prediction error $\left(\sigma_{pix}/\hat{B}_{pix}\right)$ will be 48.7% instead of 54.1%. So, our study shows that the AGB estimation and prediction errors can be underestimated by a moderate amount if the plot-level AGB uncertainty is ignored in the lidar-biomass modeling.

5 . Conclusions

The major contribution of this study is to introduce an analytical framework of characterizing AGB prediction errors by considering errors in the whole workflow of AGB mapping, including allometric model development, tree measurements, tree-level AGB prediction, plot-level AGB estimation, plot-level lidar-biomass model development, plot-level lidar metrics generation, and pixel-level AGB prediction. Our implementation of model development, for both allometric and lidar-biomass models, and error characterization using the GLS method enables us to estimate three important AGB prediction uncertainties simultaneously: 1) uncertainty related to model residuals, 2) uncertainty related to predictors (tree measurements or lidar metrics), and 3) uncertainty related to model parameters. Our method is not only useful for the remote sensing mapping community but also for researchers who use solely forest plots for AGB estimation (e.g., using large-area forest inventory plots for estimating mean AGB and its errors over an area). The application of our uncertainty analysis framework to tropical forests sites in Ghana indicates that the AGB prediction uncertainty is larger than 20% at 1 ha spatial resolution, much larger than the 10% goal proposed in previous studies. This calls for more studies in AGB estimation and mapping over tropical forests in Africa. This study also highlights the importance of considering the plot-level AGB estimate uncertainty when field plots are used to calibrate remote sensing based biomass models.

Acknowledgments

We acknowledge the ERC grant Africa GHG #247349. Great thanks are extended to Dr. Ronald McRoberts and two anonymous reviewers for their very constructive comments in improving the manuscript. The Matlab codes for GLS model fitting and AGB uncertainty analysis are available from the lead-author upon request.

Appendix 1. Generalized least squares (GLS) method for model fitting

Eqs. (3)–(7) can be solved iteratively as follows:

1) Fit a nonlinear model for Eqs. (3) and (7) to obtain an initial estimate of the allometry model parameter, $\boldsymbol{\beta}^{(0)}$, by assuming the residuals ε_{tree} are constant.
2) Obtain an initial maximum likelihood estimate of the model residual parameter $\theta^{(0)}$ by minimizing the objective function L_{tree}:

$$L_{tree}=\sum_{i=1}^{n_{tree}}\left(\frac{\left(B_{tree,i}-f_{tree}\left(\boldsymbol{\beta}^{(0)},\boldsymbol{x}_i\right)\right)^2}{2\times\left(\theta f_{tree}\left(\boldsymbol{\beta}^{(0)},\boldsymbol{x}_i\right)\right)^2}+\log\left(\theta f_{tree}\left(\boldsymbol{\beta}^{(0)},\boldsymbol{x}_i\right)\right)\right) \quad \text{(A1)}$$

where n_{tree} is the number of trees that are used to develop the allometry model (for the Chave14 database, $n_{tree}=4004$) and i is the index of the trees. After $\theta^{(0)}$ is obtained, it will be used along with $\boldsymbol{\beta}^{(0)}$ in Eq. (6) to estimate the standard deviation of residuals $\sigma^{(0)}_{\varepsilon,tree}$ for every tree.
3) Define a weight function w that is inversely related to $\sigma^{(0)}_{\varepsilon,tree}$ as follows:

$$w=\left(\frac{1}{\sigma^{(0)}_{\varepsilon,tree}}\right)^2=\left(\frac{1}{\theta^{(0)}f_{tree}\left(\boldsymbol{\beta}^{(0)},\boldsymbol{x}\right)}\right)^2 \quad \text{(A2)}$$

and solve Eqs. (3) and (7) using the nonlinear weighted least squares method (Brown et al., 1989) to get updated estimates of the parameter $\boldsymbol{\beta}^{(1)}$.
4) Repeat steps 2) and 3) until convergence. The final estimated model parameters are denoted as $\hat{\boldsymbol{\beta}}$ and $\hat{\theta}$.

Appendix 2. Standard error of predicted tree AGB mean

With linear approximation, the standard error $\sigma_{f,tree}$ of the predicted AGB mean for a tree can be calculated from:

$$\sigma_{f,tree}{}^2\approx\sum_{j=1}^{p}\sum_{k=1}^{p}\frac{\partial f}{\partial\beta_j}\frac{\partial f}{\partial\beta_k}\operatorname{cov}\left(\hat{\beta}_j,\hat{\beta}_k\right)\approx\sum_{j=1}^{p}\sum_{k=1}^{p}\frac{\partial f}{\partial\beta_j}\frac{\partial f}{\partial\beta_k}\frac{S}{n_{tree}-p}C^{-1}_{jk} \quad \text{(A3)}$$

$$S=\sum_{i=1}^{n_{tree}}w_i\left(B_{tree,i}-f_{tree}\left(\hat{\boldsymbol{\beta}},\boldsymbol{x}_i\right)\right)^2 \quad \text{(A4)}$$

$$C_{jk}=\sum_{i=1}^{n_{tree}}w_i\frac{\partial f}{\partial\beta_j}\frac{\partial f}{\partial\beta_k} \quad \text{(A5)}$$

where n_{tree} is the number of trees that are used to develop the allometry model ($n_{tree}=4004$ for the Chave14 database), i is the index of the trees, $f_{tree}\left(\hat{\boldsymbol{\beta}},\boldsymbol{x}_i\right)$ is the allometric model with parameter $\hat{\boldsymbol{\beta}}$, w_i is defined in Eq. (A4) for every tree i, C is the $p\times p$ ($p=$ the number of allometry model parameters $\hat{\boldsymbol{\beta}}$, which is 2 in our case) square matrix. Note that the partial derivative $\partial f/\partial\beta$ in Eq. (A5) is calculated for every tree i in the Chave14 database while the partial derivative in Eq. (A3) is for a new tree in our Ghana study site, so $\sigma_{f,tree}$ is a function of the new tree's attributes $\boldsymbol{x}$.

Appendix 3. Error of predicting tree AGB when a tree has measurement errors in $\boldsymbol{x}$

When both AGB errors σ_ε and σ_f (related to model residuals and parameters, respectively) are considered, the AGB of a tree is:

$$B_{tree}=f_{tree}(\boldsymbol{\beta},\boldsymbol{x})+\sigma_{\varepsilon,tree}\xi_\varepsilon+\sigma_{f,tree}\xi_f \quad \text{(A6)}$$

where both ξ_ε and ξ_f are independent standard random variables.

The three terms at the right hand side of the above equation are independent, so we have:

$$\operatorname{var}(B_{tree})=\operatorname{var}(f_{tree}(\boldsymbol{\beta},\boldsymbol{x}))+\operatorname{var}\left(\sigma_{\varepsilon,tree}\xi_\varepsilon\right)+\operatorname{var}\left(\sigma_{f,tree}\xi_f\right) \quad \text{(A7)}$$

Also we can derive that:

$$\mathrm{var}\left(\sigma_{\varepsilon,tree}\xi_{\varepsilon}\right) = \mathrm{var}(\theta f_{tree}(\boldsymbol{\beta},\boldsymbol{x})\xi_{\varepsilon}) = \theta^2\left(\mathrm{var}(f_{tree}(\boldsymbol{\beta},\boldsymbol{x})) + (f_{tree}(\boldsymbol{\beta},\boldsymbol{x}))^2\right) \tag{A8}$$

$$\mathrm{var}\left(\sigma_{f,tree}\xi_{f}\right) = \mathrm{var}\left(\sigma_{f,tree}\right) + {\sigma_{f,tree}}^2 \tag{A9}$$

where $\mathrm{var}(\sigma_{f,tree})$ is the variance of $\sigma_{f,tree}$ caused by $\boldsymbol{x}$ errors.

Combine the above three equations, and we have:

$$\mathrm{var}(B_{tree}) = {\sigma_{\varepsilon,tree}}^2 + {\sigma_{f,tree}}^2 + \left(\hat{\theta}^2+1\right)\mathrm{var}\left(f_{tree}\left(\hat{\boldsymbol{\beta}},\boldsymbol{x}\right)\right) + \mathrm{var}\left(\sigma_{f,tree}\right) \tag{A10}$$

Appendix 4. Revision of the GLS method for predicting plot-level biomass using lidar

To consider the uncertainty in $\hat{B}_{plot,j}$ in the GLS method, we modified the objective function of lidar-based biomass model residual parameter k as follows:

$$L_{plot} = \sum_{j=1}^{n_{plot}}\left(\frac{\left(\hat{B}_{plot,j} - f_{plot}\left(\boldsymbol{\varphi},\boldsymbol{z_j}\right)\right)^2 + \sigma^2_{\hat{B}_{plot,j}}}{2\times\left(kf_{plot}\left(\boldsymbol{\varphi},\boldsymbol{z_j}\right)\right)^2} + \log\left(kf_{plot}\left(\boldsymbol{\varphi},\boldsymbol{z_j}\right)\right)\right) \tag{A11}$$

where n_{plot} is the number of field plots in Ghana used for developing lidar-based biomass model ($n_{plot} = 36$ in our study); j is the index of the field plots. Compare Eqs. (A1) and (A11), and one will see that the difference is the addition of the term, $\sigma^2_{\hat{B}_{plot,j}}$ which is the uncertainty of $\hat{B}_{plot,j}$.

Appendix 5. Equation for estimating $\sigma_{f,tree}$ related to allometric model parameter uncertainty

The variance–covariance matrix of the estimated parameters of the allometric model is:

$$\begin{bmatrix} \mathrm{var}\left(\hat{\beta}_1\right) & \mathrm{cov}\left(\hat{\beta}_1,\hat{\beta}_2\right) \\ \mathrm{cov}\left(\hat{\beta}_1,\hat{\beta}_2\right) & \mathrm{var}\left(\hat{\beta}_2\right) \end{bmatrix} = \begin{bmatrix} 2.4656\times10^{-6} & -4.217\times10^{-6} \\ -4.217\times10^{-6} & 7.7686\times10^{-6} \end{bmatrix} \tag{A12}$$

The estimated parameters are: $\hat{\beta}_1 = 0.0704, \hat{\beta}_2 = 0.9701$. According to Eq. (A3), we know that:

$$\begin{aligned} {\sigma_{f,tree}}^2 \approx & \left(\left(\rho D^2 H\right)^{0.9701}\right)^2 \times \left(2.4656\times10^{-6}\right) \\ & +0.1408\times\left(\left(\rho D^2 H\right)^{0.9701}\right)^2 \times \ln\left(\rho D^2 H\right)\times\left(-4.217\times10^{-6}\right) \\ & +\left(0.0704\times\left(\rho D^2 H\right)^{0.9701}\times\ln\left(\rho D^2 H\right)\right)^2\times7.7686\times10^{-6} \end{aligned} \tag{A13}$$

References

Achard, F., Beuchle, R., Mayaux, P., Stibig, H. J., Bodart, C., Brink, A., et al. (2014). Determination of tropical deforestation rates and related carbon losses from 1990 to 2010. *Global Change Biology*, *20*(8), 2540–2554.

Asner, G. P., Clark, J. K., Mascaro, J., Galindo García, G. A., Chadwick, K. D., Navarrete Encinales, D. A., et al. (2012). High-resolution mapping of forest carbon stocks in the Colombian Amazon. *Biogeosciences*, *9*, 2683–2696.

Asner, G. P., & Mascaro, J. (2014). Mapping tropical forest carbon: Calibrating plot estimates to a simple LiDAR metric. *Remote Sensing of Environment*, *140*, 614–624.

Baccini, A., Goetz, S. J., Walker, W. S., Laporte, N. T., Sun, M., Sulla-Menashe, D., et al. (2012). Estimated carbon dioxide emissions from tropical deforestation improved by carbon-density maps. *Nature Climate Change*, *2*(3), 182–185.

Baccini, A., Laporte, N., Goetz, S. J., Sun, M., & Dong, H. (2008). A first map of tropical Africa's above-ground biomass derived from satellite imagery. *Environmental Research Letters*, *3*(4), 045011.

Barrett, D. J., Galbally, I. E., & Graetz, R. D. (2001). Quantifying uncertainty in estimates of C emissions from above-ground biomass due to historic land-use change to cropping in Australia. *Global Change Biology*, *7*(8), 883–902.

Bates, D. M., & Watts, D. G. (1988). *Nonlinear regression analysis and its applications*. John Wiley & Sons, Inc.

Berenguer, E., Ferreira, J., Gardner, T. A., Aragão, L. E. O. C., De Camargo, P. B., Cerri, C. E., et al. (2014). A large-scale field assessment of carbon stocks in human-modified tropical forests. *Global Change Biology*. http://dx.doi.org/10.1111/gcb.12627.

Berger, A., Gschwantner, T., McRoberts, R. E., & Schadauer, K. (2014). Effects of measurement errors on individual tree stem volume estimates for the Austrian National Forest Inventory. *Forest Science*, *60*(1), 14–24.

Bonan, G. B. (2008). Forests and climate change: Forcings, feedbacks, and the climate benefits of forests. *Science*, *320*, 1444–1449.

Breidenbach, J., Antón-Fernández, C., Petersson, H., McRoberts, R. E., & Astrup, R. (2014). Quantifying the model-related variability of biomass stock and change estimates in the Norwegian national forest inventory. *Forest Science*, *60*(1), 25–33.

Brown, S., Gillespie, A. J., & Lugo, A. E. (1989). Biomass estimation methods for tropical forests with applications to forest inventory data. *Forest Science*, *35*(4), 881–902.

Chave, J., Condit, R., Aguilar, S., Hernandez, A., Lao, S., & Perez, R. (2004). Error propagation and scaling for tropical forest biomass estimates. *Philosophical Transactions of the Royal Society of London. Series B, Biological Sciences*, *359*(1443), 409–420.

Chave, J., Coomes, D., Jansen, S., Lewis, S. L., Swenson, N. G., & Zanne, A. E. (2009). Towards a worldwide wood economics spectrum. *Ecology Letters*, *12*(4), 351–366.

Chave, J., Réjou-Méchain, M., Búrquez, A., Chidumayo, E., Colgan, M. S., Delitti, W. B., et al. (2014). Improved allometric models to estimate the aboveground biomass of tropical trees. *Global Change Biology*. http://dx.doi.org/10.1111/gcb.12629.

Chen, Q. (2007). Airborne lidar data processing and information extraction. *Photogrammetric Engineering and Remote Sensing*, *73*(2), 109–112.

Chen, Q. (2010). Retrieving vegetation height of forests and woodlands over mountainous areas in the Pacific Coast region using satellite laser altimetry. *Remote Sensing of Environment*, *114*(7), 1610–1627.

Chen, Q. (2013). *Lidar remote sensing of vegetation biomass. Remote sensing of natural resources*. (pp. 399–420)CRC Press: Taylor & Francis, Group, 399–420.

Chen, Q., Vaglio Laurin, G., Battles, J. J., & Saah, D. (2012). Integration of airborne lidar and vegetation types derived from aerial photography for mapping aboveground live biomass. *Remote Sensing of Environment*, *121*, 108–117.

Clark, D. B., & Kellner, J. R. (2012). Tropical forest biomass estimation and the fallacy of misplaced concreteness. *Journal of Vegetation Science*, *23*(6), 1191–1196.

Clark, M. L., Roberts, D. A., Ewel, J. J., & Clark, D. B. (2011). Estimation of tropical rain forest aboveground biomass with small-footprint lidar and hyperspectral sensors. *Remote Sensing of Environment*, *115*(11), 2931–2942.

DeFries, R., Achard, F., Brown, S., Herold, M., Murdiyarso, D., & Schlamadinger, B. (2007). Earth observations for estimating greenhouse gas emissions from deforestation in developing countries. *Environmental Science & Policy*, *10*(4), 385–394.

Dubayah, R. O., Sheldon, S. L., Clark, D. B., Hofton, M. A., Blair, J. B., & Chazdon, R. L. (2010). Estimation of tropical forest height and biomass dynamics using lidar remote sensing at La Selva, Costa Rica. *Journal of Geophysical Research, G: Biogeosciences*, *115*, GE00E09.

Gertner, G., Cao, X., & Zhu, H. (1995). A quality assessment of a Weibull based growth projection system. *Forest Ecology and Management*, *71*(3), 235–250.

Goetz, S. J., Baccini, A., Laporte, N. T., Johns, T., Walker, W., Kellndorfer, J., et al. (2009). Mapping and monitoring carbon stocks with satellite observations: A comparison of methods. *Carbon Balance and Management*, *4*(1).

Gonzalez, P., Asner, G. P., Battles, J. J., Lefsky, M. A., Waring, K. M., & Palace, M. (2010). Forest carbon densities and uncertainties from Lidar, QuickBird, and field measurements in California. *Remote Sensing of Environment*, *114*(7), 1561–1575.

Grace, J., Mitchard, E., & Gloor, E. (2014). Perturbations in the carbon budget of the tropics. *Global Change Biology*. http://dx.doi.org/10.1111/gcb.12600.

Gregoire, T. G., Ståhl, G., Næsset, E., Gobakken, T., Nelson, R., & Holm, S. (2010). Model-assisted estimation of biomass in a LiDAR sample survey in Hedmark County, Norway. *Canadian Journal of Forest Research*, *41*(1), 83–95.

Houghton, R. A., Lawrence, K. T., Hackler, J. L., & Brown, S. (2001). The spatial distribution of forest biomass in the Brazilian Amazon: A comparison of estimates. *Global Change Biology*, *7*(7), 731–746.

Hunter, M. O., Keller, M., Vitoria, D., & Morton, D. C. (2013). Tree height and tropical forest biomass estimation. *Biogeosciences*, *10*, 8385–8399.

Lu, D., Chen, Q., Wang, G., Liu, L., Li, G., & Moran, E. (2014). A survey of remote sensing-based aboveground biomass estimation methods in forest ecosystems. *International Journal of Digital Earth*. http://dx.doi.org/10.1080/17538947.2014.990526.

Mascaro, J., Detto, M., Asner, G. P., & Muller-Landau, H. C. (2011). Evaluating uncertainty in mapping forest carbon with airborne LiDAR. *Remote Sensing of Environment*, *115*(12), 3770–3774.

McRoberts, R. E., & Westfall, J. A. (2014). Effects of uncertainty in model predictions of individual tree volume on large-area volume estimates. *Forest Science*, *60*(1), 34–42.

Mitchard, E. T., Saatchi, S. S., Baccini, A., Asner, G. P., Goetz, S. J., Harris, N., et al. (2013). Uncertainty in the spatial distribution of tropical forest biomass: A comparison of pan-tropical maps. *Carbon Balance and Management*, *8*(10), 1–13.

Ometto, J. P., Aguiar, A. P., Assis, T., Soler, L., Valle, P., Tejada, G., et al. (2014). Amazon forest biomass density maps: Tackling the uncertainty in carbon emission estimates. *Climatic Change*, *124*(3), 545–560.

Phillips, D. L., Brown, S. L., Schroeder, P. E., & Birdsey, R. A. (2000). Toward error analysis of large-scale forest carbon budgets. *Global Ecology and Biogeography*, *9*(4), 305–313.

Saatchi, S. S., Harris, N. L., Brown, S., Lefsky, M., Mitchard, E. T., Salas, W., et al. (2011). Benchmark map of forest carbon stocks in tropical regions across three continents. *Proceedings of the National Academy of Sciences*, *108*(24), 9899–9904.

Ståhl, G., Heikkinen, J., Petersson, H., Repola, J., & Holm, S. (2014). Sample-based estimation of greenhouse gas emissions from forests—A new approach to account for both sampling and model errors. *Forest Science*, *60*(1), 3–13.

Vaglio Laurin, G., Chen, Q., Lindsell, J. A., Coomes, D. A., Frate, F. D., Guerriero, L., et al. (2014). Above ground biomass estimation in an African tropical forest with lidar and hyperspectral data. *ISPRS Journal of Photogrammetry and Remote Sensing*, *89*, 49–58.

Wang, G., Oyana, T., Zhang, M., Adu-Prah, S., Zeng, S., Lin, H., et al. (2009). Mapping and spatial uncertainty analysis of forest vegetation carbon by combining national forest inventory data and satellite images. *Forest Ecology and Management*, *258*(7), 1275–1283.

Yanai, R. D., Battles, J. J., Richardson, A. D., Blodgett, C. A., Wood, D. M., & Rastetter, E. B. (2010). Estimating uncertainty in ecosystem budget calculations. *Ecosystems*, *13*(2), 239–248.

Zolkos, S. G., Goetz, S. J., & Dubayah, R. (2013). A meta-analysis of terrestrial aboveground biomass estimation using lidar remote sensing. *Remote Sensing of Environment*, *128*, 289–298.